

On Nanowire Morphological Instability and Pinch-Off by Surface Electromigration

Mikhail Khenner^{a1,2}

¹*Department of Mathematics, Western Kentucky University, Bowling Green, KY 42101, USA*

²*Applied Physics Institute, Western Kentucky University, Bowling Green, KY 42101, USA*

(Dated: November 8, 2024)

Surface diffusion and surface electromigration may lead to a morphological instability of thin solid films and nanowires. In this paper two nonlinear analyses of a morphological instability are developed for a single-crystal cylindrical nanowire that is subjected to an axial current. These treatments extend the conventional linear stability analyses without surface electromigration, that manifest a Rayleigh-Plateau instability. A weakly nonlinear analysis is done slightly above the Rayleigh-Plateau (longwave) instability threshold. It results in a one-dimensional Sivashinsky amplitude equation that describes a blow-up of a surface perturbation amplitude in a finite time. This is a signature of a pinching singularity of a cylinder radius, which leads to a wire separation into a disjoint segments. The time- and electric field-dependent dimensions of the focusing self-similar amplitude profile approaching a blow-up are characterized via the scaling analysis. Also, a weakly nonlinear multi-scale analysis is done at the arbitrary distance above a longwave or a shortwave instability threshold. The time- and electric field-dependent Fourier amplitudes of the major instability modes are derived and characterized.

Keywords: Nanowires, morphological stability, electromigration, singular solutions of PDEs, weakly nonlinear analysis, scaling analysis, multi-scale analysis

I. INTRODUCTION

Surface electromigration [1–3] is a well-known and efficient method to guide morphological changes of thin films by surface diffusion. In particular, it has been used to manufacture nanocontacts by breaking of thin films and nanowires via a controlled pinch-offs [4–6]. Such nanocontacts are required for engineering and biomedical applications, for example, for measurement of the electrical conductance and electronic properties of a molecule, but forming a quality nanocontact is still a major challenge [7]. To overcome that challenge, the first step should be a basic understanding of a surface electromigration-driven morphological instability of a single-crystal wire that leads to a pinch-off event.

Modeling morphological instabilities of nanowires by a classical approach of accounting for surface diffusion via an evolution partial differential equation (PDE) for a shape variable [8–10] flourished in the 1990s and early 2000s [11–17]. A recent paper emphasizing this approach is by Wang *et al.* [18]. These authors considered a surface area minimization problem, computed a wire pinch-off using a phase-field method, and extended the Rayleigh-Plateau stability condition to finite amplitude perturbations. Also limited Monte Carlo computations were published [19]. For predictive applied modeling of a nanocontact fabrication process a multi-physics framework is needed, that explicitly includes a model and a computation of a nanowire pinch-off instability, whereby the latter is triggered and enhanced by the surface current. Since the cited works do not consider the key mass transport mechanism, namely surface electromigration (shortened to electromigration in the rest of the paper), they cannot form a basis for that framework.

Toward the stated goal, in Ref. [20] this author introduced a PDE-based model for electromigrated cylindrical nanowire deposited on a substrate. That model is complicated by the presence of the contact lines and a non-axisymmetric surface instability modes. A linear stability analysis (LSA) of that model is performed in Ref. [20], from which a simpler case of axisymmetrically evolving free-standing wire is easily recovered. Axisymmetric modes dominate evolution of surface perturbations for a free-standing wire in the absence of electromigration, i.e. when only a natural high-temperature surface diffusion is operative [11]. Provided the axial current and a corresponding diffusion anisotropy that is a function of the axial variable, this is expected to hold when the electromigration is also operative. Ref. [21] reports a computation of a wire breakup into a chain set of particles for the simpler case. The breakup time and the number of particles that emerge upon a breakup are characterized as a function of the initial surface roughness.

In this communication, also assuming axisymmetrically evolving, free-standing long wire, in Sec. III we perform a weakly nonlinear analysis slightly above the longwave instability threshold. The latter means that a critical (a most dangerous, i.e. a fastest growing) sinusoidal perturbation of a uniform surface profile $r(y) = \text{const.}$ (where r is a wire radius and y the axial coordinate) has a tiny axial wavenumber $k \rightarrow 0$. We derive an amplitude equation via the expansion of a governing PDE up to the terms that are quadratic in the amplitude, whereas LSA is based on the

^a Corresponding author. E-mail: mikhail.khenner@wku.edu.

expansion up to linear terms, i.e. a linearization procedure. In other words, the perturbation amplitude is finite in the weakly nonlinear analysis. This key underlying assumption is the same in this paper and in Ref. [18]. A finite amplitude is quite likely to occur in experiment [22]. A scaling analysis and a computation of the amplitude equation show that the amplitude becomes unbounded (blows up) in finite time. Following Ref. [23] and to simplify writing, we will refer to the amplitude approaching a blow-up singularity as a spike. From the analysis we obtain the much needed information on the time-and-electric field-dependent dimensions of the spike. Note that the blow-up singularity of the amplitude (a spike formation) is the signature of a finite-time pinching singularity of a wire radius ($r \rightarrow 0$). The (finite) time of a singularity formation is the same for the amplitude singularity and for the radius singularity. In a basic experiment demonstrating a Rayleigh-Plateau instability without electromigration a wire pinches off at multiple locations along the axis, thus several shorter cylindrical wire segments are formed [24, 25]. The spacing between pinch-offs is approximately equal to the most dangerous wavelength. Depending on a new segment's length (that is, depending on whether a Rayleigh-Plateau instability is again operational) a segment may further pinch-off resulting in even shorter segments, or, provided sufficient time, it may transform by surface diffusion into a spherical nanoparticle.

Independent of the weakly nonlinear analysis, in Sec. IV we start with the assumption of the initial unstable surface perturbation having an arbitrary finite wavenumber $0 < k < k_c$, where k_c is the instability cut-off wavenumber from LSA, and ask which unstable surface modes are the fastest growing. In this weakly nonlinear multi-scale treatment the spike formation is not considered. (As in the “standard” weakly nonlinear analysis in Sec. III, the governing PDE for the surface variable will be expanded to second order in a small parameter that has a meaning of a perturbation amplitude. This explains why we use the term “weakly nonlinear multi-scale analysis”.) Nonlinearity of the governing PDE forces a fast distortion of the initial sinusoidal surface perturbation into a general smooth surface shape, and as was just explained, we are interested in finding the fastest growing Fourier modes in its spectrum.

II. THE MODEL

We consider surface electromigration on a free-standing cylindrical nanowire of radius R_0 . (For details of the model derivation, see Ref. [20].) Assuming axial symmetry and a constant electric field E_0 in the axial direction, the wire radius $r(t, y)$ is governed by a nonlinear dimensionless evolution PDE:

$$r_t = \frac{1}{r} \frac{\partial}{\partial y} \left[M(r_y) \frac{r K_y + E}{\sqrt{1 + r_y^2}} \right], \quad (1)$$

where y is the axial variable,

$$K = \frac{1}{r \sqrt{1 + r_y^2}} - \frac{r_{yy}}{(1 + r_y^2)^{3/2}} \quad (2)$$

the mean curvature of the surface, and

$$M(r_y) = \frac{1 + S \cos^2(\arctan r_y + \psi)}{1 + S} \quad (3)$$

the anisotropic diffusional mobility of the adsorbed atoms (adatoms) [26]. Here $S > 0$ is the anisotropy strength and $0 \leq \psi \leq \pi/2$ the misorientation angle for a wire oriented along the [100] crystallographic direction. Also $E = Q\Delta V R_0^2 / (\Omega \gamma \ell)$ is the electric field parameter, where $Q > 0$ is the effective charge of ionized adatoms, ΔV a voltage difference between the front and back faces of a wire, ℓ the wire length, Ω the atomic volume, and γ the surface energy. Note that $E_0 = \Delta V / \ell$, and thus a positivity (a negativity) of E_0 and E depends on the sign of ΔV . When surface diffusion is isotropic ($S = 0 \rightarrow M(r_y) = 1$) and the electric field is off ($E = 0$), Eq. (1) reduces to a well-known evolution equation $r_t = \frac{1}{r} \frac{\partial}{\partial y} \left[\frac{r K_y}{(1 + r_y^2)^{1/2}} \right]$ [11, 12], which expresses only the adatom surface diffusion via a surface Laplacian of mean curvature.

A. Linear Stability Analysis

Eq. (1) has the trivial solution $r = 1$ (the base state), corresponding to unperturbed cylinder. Introducing a tiny perturbation of the base state, $r = 1 + \xi_0 e^{\sigma t} \cos ky$, $\xi_0 \ll 1$, and linearizing in ξ_0 gives the growth rate σ and the

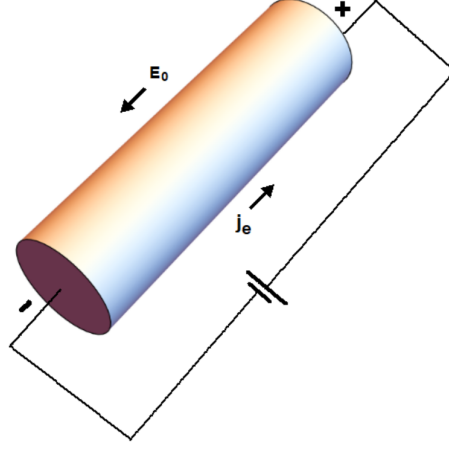


FIG. 1. Unperturbed cylindrical nanowire (the base state). j_e is the surface electric current that drives the surface electromigration of adatoms via the "electron wind" [1–3].

instability cut-off wavenumber k_c [20]:

$$\sigma(k; E) = \frac{2 + S(1 + \cos 2\psi)}{2(1 + S)} k^2 (1 - k^2) + E \frac{S \sin 2\psi}{1 + S} k^2 \equiv \frac{\alpha_1 + \alpha_3}{2(\alpha_3 - 1)} k^2 (1 - k^2) + \frac{\alpha_2}{\alpha_3 - 1} E k^2, \quad (4)$$

$$k_c(E) = \sqrt{1 + \frac{2SE \sin 2\psi}{2 + S(1 + \cos 2\psi)}} \equiv \sqrt{1 + \frac{2\alpha_2 E}{\alpha_1 + \alpha_3}}. \quad (5)$$

Perturbations with a wavenumbers $0 < k < k_c(E)$ destabilize the base state, since for these wavenumbers $\sigma(k; E) > 0$. This is a longwave instability. Here we introduced a non-negative parameters $\alpha_1 = S \cos 2\psi$, $\alpha_2 = S \sin 2\psi$ and a positive parameter $\alpha_3 = 2 + S$. At $S = 0$ (isotropy) with either $E = 0$, or $E \neq 0$, Eqs. (4) and (5) reduce to $\sigma(k; 0) = k^2(1 - k^2)$ and $k_c(0) = 1$, respectively, which characterize a classical Rayleigh-Plateau instability of a free-standing solid wire [8]. In dimensional coordinates this implies that an axisymmetric sinusoidal perturbation induces instability if and only if its wavelength is longer than the circumference of the undisturbed cylinder.

Setting $\sigma = 0$ results in the neutral stability curve $E(k) = \frac{\alpha_1 + \alpha_3}{2\alpha_2} (k^2 - 1)$. Fig. 2 shows this curve for $S = 1$ and $\psi = \pi/12$ [20] (these values are fixed for the remainder of this paper). The threshold of a longwave instability is

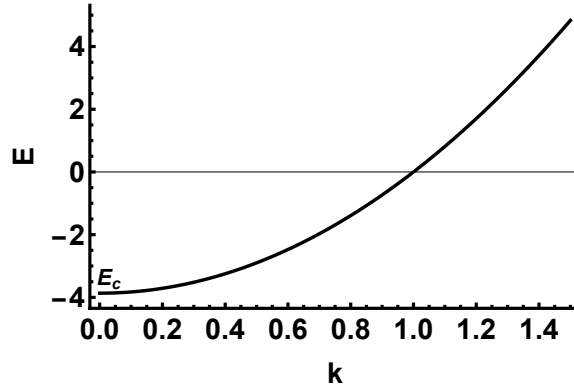


FIG. 2. The neutral stability curve $E(k)$.

$(k, E_c) = (0, \frac{-(\alpha_1 + \alpha_3)}{2\alpha_2}) = (0, -3.866)$. Above the neutral stability curve, i.e. for $E > E_c$ the wire is unstable; below the neutral stability curve it is stable. For $E > 0$ the instability is due to a combined action of two destabilizing factors, the electromigration and a surface diffusion. For $E < E_c$ the wire is completely stabilized by electromigration. For $E_c < E < 0$ the stabilizing action of electromigration is weak and the instability due to surface diffusion still emerges. Fig. 3 shows why not only the strength of the electric field, but also its direction (determined by a sign of ΔV) matters for a morphological instability.

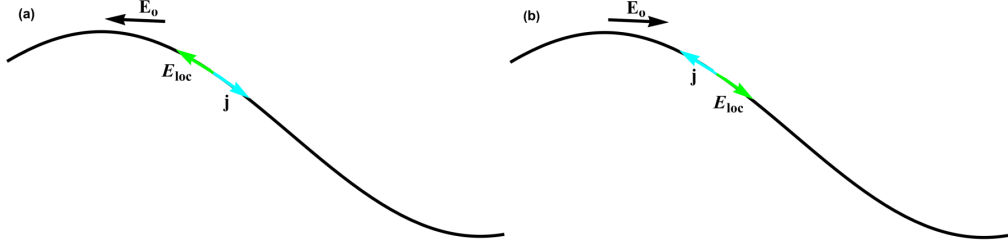


FIG. 3. (a,b) Sketch of a cross-section of a bump on a wire surface by a plane that is parallel to a wire axis. A projection of a constant electric field E_0 onto a surface, E_{loc} , drives the electromigration adatom flux j in the opposite direction, i.e. in the direction of the electron flow j_e . This contributes to either (a) a bump smoothing (stabilization), or to (b) a bump growth (destabilization).

Remark. In Ref. [18], where electromigration is not considered, a correction to $k_c(0)$ is derived that accounts for the finite perturbation amplitude, i.e. the starting assumption $\xi_0 \ll 1$ is replaced by $0 < \xi_0 < 1$. The corrected expression reads $k_c(0) = \sqrt{1 + \xi_0^2}$. For the analyses that follow in Sections III and IV it is not necessary to likewise correct k_c in Eq. 5, since in Sec. III $k \rightarrow 0$ (is tiny) and k_c is irrelevant, and in Sec. IV k_c is not needed explicitly.

III. WEAKLY NONLINEAR ANALYSIS SLIGHTLY ABOVE THE INSTABILITY THRESHOLD (k, E) = (0, E_c)

We start by substituting $r = 1 + \delta\xi(t, y)$, $\delta \ll 1$ in the right-hand side of Eq. (1), expanding to second order in δ , and formally adding the coefficients of δ and δ^2 . This results in:

$$\begin{aligned}
 (\alpha_3 - 1) \xi_t = & - \left(E\alpha_2 + \frac{1}{2}(\alpha_1 + \alpha_3) \right) \xi_{yy} - \frac{1}{2}(\alpha_1 + \alpha_3) \xi_{yyy} + \frac{1}{2}(\alpha_1 + \alpha_3) \xi_y^2 - \frac{1}{2}(\alpha_1 + \alpha_3) \xi_{yy}^2 \\
 & - (\alpha_1 + \alpha_3) \xi_y \xi_{yyy} + \left[(E\alpha_2 + \alpha_1 + \alpha_3) \xi + \left(2\alpha_2 - \frac{1}{2}E(5\alpha_1 + \alpha_3) \right) \xi_y + \alpha_2 \xi_{yyy} \right] \xi_{yy} + \alpha_2 \xi_y \xi_{yyy}. \quad (6)
 \end{aligned}$$

LSA results (4), (5) may be recovered from Eq. (6).

Let $E = E_c + \epsilon E_1$, $E_1 = \mathcal{O}(1) > 0$. Note that the coefficient of ξ_{yy} changes its sign at $E = E_c$, hence it is proportional to $E - E_c = \epsilon E_1$, which is $\mathcal{O}(\epsilon)$. The balance of the largest nonlinear term $\sim \xi_y^2$ with the linear term $\sim \epsilon \xi_{yy}$ is for $\xi(t, y) = \epsilon \phi(t, y)$, $\phi = \mathcal{O}(1)$. Also, since the linear instability interval is $0 < k < k_c$, where $k_c = \sqrt{1 + \frac{2\alpha_2 E}{\alpha_1 + \alpha_3}} = \sqrt{1 - \frac{E}{E_c}} = \sqrt{\frac{-E_1}{E_c}} \epsilon = \mathcal{O}(\epsilon^{1/2})$, the appropriate rescaling of the axial coordinate y is $Y = \epsilon^{1/2} y$.

Thus also let:

$$\xi = \epsilon \phi; \quad T = \epsilon^2 t \Leftrightarrow \partial_t = \epsilon^2 \partial_T, \quad Y = \epsilon^{1/2} y \Leftrightarrow \partial_y = \epsilon^{1/2} \partial_Y, \quad (7)$$

where T, Y are a slow time and a stretched axial variable.

Inserting $E = E_c + \epsilon E_1$ and expansions (7) in Eq. (6) we get:

$$\phi_T \epsilon^3 = - \left\{ \alpha_2 E_c + \frac{1}{2}(\alpha_1 + \alpha_3) \right\} \phi_{YY} \epsilon^2 + \{ -a \phi_{YY} - b [\phi_{YYYY} - \phi_Y^2 - \phi \phi_{YY}] \} \epsilon^3 + \mathcal{O}(\epsilon^{7/2}), \quad (8)$$

where $a = \frac{\alpha_2 E_1}{\alpha_3 - 1} = \frac{S E_1 \sin 2\psi}{1 + S} = E_1/4 > 0$, $b = \frac{\alpha_1 + \alpha_3}{2(\alpha_3 - 1)} = \frac{2 + S(1 + \cos 2\psi)}{2(1 + S)} \approx 0.966$. Noticing that the coefficient of $\phi_{YY} \epsilon^2$ is zero, in the lowest order ϵ^3 we finally obtain the amplitude equation

$$\phi_T = -a \phi_{YY} - b [\phi_{YYYY} - \phi_Y^2 - \phi \phi_{YY}]. \quad (9)$$

Eq. (9) can be also written in the form:

$$\phi_T = -a \phi_{YY} - b \phi_{YYYY} + \frac{1}{2} b \partial_{YY} \phi^2. \quad (10)$$

Introducing the scalings of Y and T :

$$X = \sqrt{\frac{a}{2b}}Y \Leftrightarrow \partial_Y = \sqrt{\frac{a}{2b}}\partial_X, \quad \tau = \frac{a^2}{2b}T \Leftrightarrow \partial_T = \frac{a^2}{2b}\partial_\tau \quad (11)$$

eliminates one parameter from Eq. (10) and results in equation that has the form of Eq. (9) in Ref. [23]:

$$\phi_\tau = -\phi_{XX} - \frac{1}{2}\phi_{XXX} + c \partial_X \phi^2, \quad c = \frac{b}{2a}. \quad (12)$$

Letting $\phi = h_X$ in Eq. (12) gives equation

$$h_\tau = -h_{XX} - \frac{1}{2}h_{XXX} + c \partial_X h_X^2, \quad (13)$$

that has the form of Eq. (8) in Ref. [23]. LSA of Eqs. (12) and (13) about the base states $\phi = 1$ and $h_X = 1$, respectively, give the perturbation growth rate $\sigma = (1 - 2c)k^2 - \frac{k^4}{2}$. Thus these base states are longwave unstable at $0 < c < 1/2 \Leftrightarrow 0 < b/a < 1$, with the instability cut-off wavenumber $k_c = \sqrt{2(1 - 2c)}$.

Notice that setting $\phi = w_{XX}, c = 1$ in Eq. (12) and integrating twice with respect to X gives $w_\tau = -w_{XX} - w_{XXXX} + w_{XX}^2$ [27]. This equation was rigorously studied in Ref. [28] (see equation (1D MKS) on p. 377 of that paper, which reads $w_\tau = -w_{XX} - w_{XXXX} + (1 - \lambda)w_X^2 + \sigma\lambda w_{XX}^2$, with $\lambda = \sigma = 1$). For the 1D MKS equation on a periodic domain these authors proved that depending on the stability of the trivial solution, either: (i) if it is unstable, there exist arbitrarily small initial perturbations that lead to a solution blow-up in a finite time, or (ii) if it is stable, there exist finite-amplitude initial perturbations that lead to a finite-time blow-up. These singularities exhibit self-similar structure in w_{XX} . Their numerical results indicated that w generically becomes pointwise infinite at a finite time. Notice that the limit $\lambda \rightarrow 0$ recovers the Kuramoto-Sivashinsky equation which does not exhibit blow-up in one dimension. Also, Eq. (12) with the -1 coefficient of ϕ_{XXX} and $c = -1$ has been studied in Ref. [29]. For that equation (the Sivashinsky equation) these authors found an infinite family of self-similar blow-up solutions, performed their LSA, and identified a unique stable blow-up solution. We will refer to Eq. (12) also as Sivashinsky equation.

A convenient scaling analysis of a solution singularity development for Eq. (12) (and Eq. (13)) was performed in Ref. [23]. For the sake of clarity we repeat the major points of this analysis below, using our notation.

Let the singularity forms at location $X = 0$ at time $\tau = \tau_s$. For $|X| \ll 1$ and $\tau \lesssim \tau_s$, the variable h varies rapidly with position and h_{XX} is negligible compared to h_{XXX} . Therefore when seeking the behavior of h close to the singularity, one may consider Eq. (13) without the term $-h_{XX}$. Next, rescaling the distance $\tilde{X} = cX$ and time $\tilde{\tau} = c^4\tau$ gives

$$h_{\tilde{\tau}} = -\frac{1}{2}h_{\tilde{X}\tilde{X}\tilde{X}} + \partial_{\tilde{X}} h_{\tilde{X}}^2. \quad (14)$$

One seeks similarity solutions to this equation that have the form

$$h(\tilde{\tau}, \tilde{X}) = \frac{1}{(\tilde{\tau}_s - \tilde{\tau})^{\gamma_1}} G\left(\frac{\tilde{X} - \bar{X}}{(\tilde{\tau}_s - \tilde{\tau})^{\gamma_2}}\right), \quad (15)$$

where $\bar{X} = \bar{X}(\tilde{\tau})$ is the rescaled position of developing singularity, $\tilde{\tau}_s = c^4\tau_s$ is the rescaled time of singularity formation, $\tilde{\tau} < \tilde{\tau}_s$ and γ_1 and γ_2 are constant exponents. Next, from Eqs. (14), (15) and $\phi = h_X$ one arrives to:

$$\phi(\tau, X) = \frac{1}{c(\tau_s - \tau)^{1/2}} G'\left(\frac{X - x(\tau)}{(\tau_s - \tau)^{1/4}}\right), \quad (16)$$

where $x(\tau) = \bar{X}(\tilde{\tau})/c$. Eq. (16) signals that a downward spike in ϕ develops that is centered at the point $x(\tau)$; the depth of the spike increases as $(\tau_s - \tau)^{-1/2}$ and its width decreases as $(\tau_s - \tau)^{1/4}$ as $\tau \rightarrow \tau_s$ from below. The unscaled position of the spike's center moves with velocity $x_\tau \sim (\tau_s - \tau)^{-3/4}$.

In terms of the original variables used in Eq. (6):

$$\text{spike depth} = \frac{c_1}{(E - E_c) \sqrt{b(t_s - t)}}, \quad (17)$$

$$\text{spike width} = c_2 \sqrt{a(E - E_c)} \left(\frac{t_s - t}{b} \right)^{1/4}, \quad (18)$$

$$\text{spike center displacement from } y = 0 = \frac{c_3 \sqrt{a(E - E_c)}}{b^{1/4}} \left[t_s^{1/4} - (t_s - t)^{1/4} \right], \quad (19)$$

where the time of a singularity formation t_s and the proportionality constants $c_{1,2,3}$ can't be determined from the scaling analysis. Obviously, one expects that $t_s = t_s(E - E_c) \equiv t_s(\Delta E)$, thus Eqs. (17)-(19) show the dependence of the spike parameters on time, but not yet on ΔE . In order to find the latter functional dependence, first, we notice that the computation of Eq. (12) results in $\tau_s \sim 40$ (Fig. 4(a)). Thus using Eqs. (7) and (11):

$$t_s = \frac{2b\tau_s}{a^2\epsilon^2} = \frac{2bE_1^2\tau_s}{a^2(E - E_c)^2} = \frac{32\tau_s}{(E - E_c)^2} \sim 1300/(E - E_c)^2 \sim 1.3 \times 10^7 \quad (20)$$

at $a = 2, b = 1, E_1 = 8 \Leftrightarrow c = 1/4$ and a representative value $\Delta E = 0.01$. Evolution of the spike dimensions at these (fixed) values of ΔE and t_s is shown in Fig. 4(b). It is seen that in comparison to the singularity of the width and the displacement, the singularity of the depth develops abruptly.

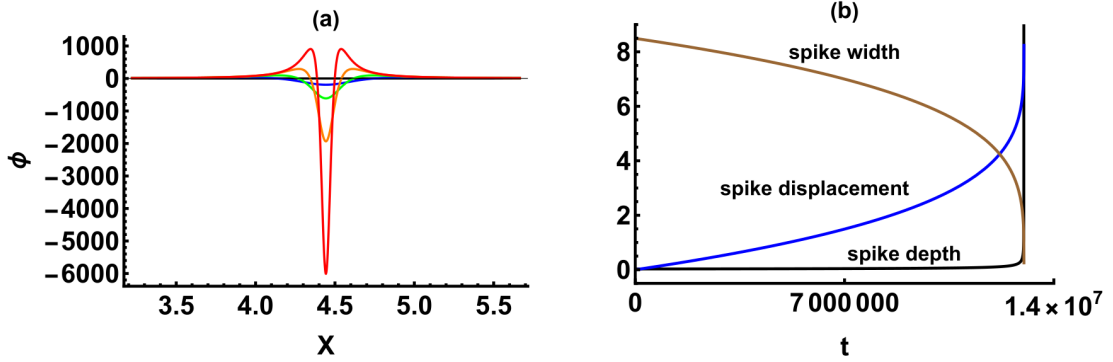


FIG. 4. (a) Spike formation via computation of Eq. (12) with $c = 1/4$. The initial condition is a small Gaussian-shaped perturbation of the base state $\phi = 1$ on the interval $0 \leq X \leq 2\sqrt{2}\pi$, where $2\sqrt{2}\pi$ is the most dangerous instability wavelength (the one at which the growth rate ω is the maximum value). Boundary conditions are periodic. The last shown profile corresponds to $\tau_s = 43.35$. (b) Evolution of the spike dimensions (Eqs. (17)-(19)) at $\Delta E = 0.01, a = 2, b = 1, E_1 = 8, t_s = 1.3 \times 10^7$. Proportionality constants $c_{1,2,3} = 1$ are chosen to facilitate plotting three functions on the same plot.

Next, inserting $t_s = 2bE_1^2\tau_s/a^2(E - E_c)^2$ in Eqs. (17)-(19) gives the following forms for the dependence of the spike parameters on ΔE and t :

$$\text{spike depth} = \frac{c_1 a}{b \sqrt{2E_1^2\tau_s - \frac{a^2(E - E_c)^2 t}{b}}}, \quad (21)$$

$$\text{spike width} = c_2 \left(2E_1^2\tau_s - \frac{a^2(E - E_c)^2 t}{b} \right)^{1/4}, \quad (22)$$

$$\text{spike center displacement from } y = 0 = c_3 \left[(2\tau_s)^{1/4} \sqrt{E_1} - \left(2E_1^2\tau_s - \frac{a^2(E - E_c)^2 t}{b} \right)^{1/4} \right]. \quad (23)$$

Figure 5 shows the major spike dimension, its depth, as the contour plot of the two-variable function (21). Spike depth increases as the time and ΔE increase. Moreover, unless the time is close to a blow-up and ΔE is not very small, the depth is more sensitive to ΔE change than to t change. This is the signature of a product $(E - E_c)^2 t$ in Eq. (21), where the exponent of t is one, and the exponent of ΔE is two. Same is true for the spike width and displacement. Also it is useful to expand Eq. (21) for small ΔE and t :

$$\text{spike depth} = \frac{c_1 a}{bE_1\sqrt{2\tau_s}} + \frac{c_1 a^3}{4\sqrt{2}b^2E_1^3\tau_s^{3/2}} (E - E_c)^2 t + O\left((E - E_c)^4 t^2\right). \quad (24)$$

This shows that the spike depth grows quadratically in ΔE and only linear in t .

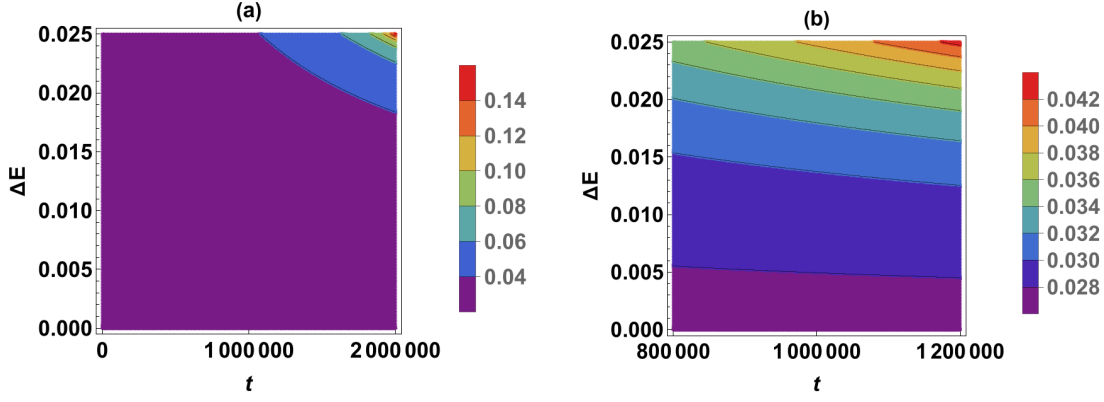


FIG. 5. Spike depth, as given by Eq. (21). $a = 2, b = 1, E_1 = 8, \tau_s = 40, c_1 = 1$. (b) is the zoom view of (a) in the middle of the time interval.

IV. A WEAKLY NONLINEAR MULTI-SCALE ANALYSIS OF THE PRIMARY MODES OF INSTABILITY

As was already noted in Introduction, due to the nonlinearity of a governing PDE (1) very shortly after the initiation of a morphological instability the initial sinusoidal, single-harmonic form of a solution (the initial condition) ceases to exist, and the solution is represented by a Fourier series. Without loss of generality, we will account only for a handful of major terms in that series, i.e. the sinusoidal terms having a wavenumbers that are a small integer multiples of a wavenumber of the primary mode (the sinusoidal initial condition/perturbation) [18], and derive their time-dependent amplitudes. The primary mode has a finite wavenumber $0 < k < k_c$.

We start with the following ansatz for the perturbation of the base state $r = 1$:

$$r = 1 + \epsilon r_1(t_0, t_1, t_2; E) \cos ky + \epsilon r_4(t_0, t_1, t_2; E) \sin ky + \epsilon^2 r_2(t_0, t_1, t_2; E) \cos 2ky + \epsilon^2 r_3(t_0, t_1, t_2; E) \sin 2ky, \quad \epsilon \ll 1 \quad (25)$$

where t_0 is the fast time and t_1, t_2 are the slow times. Thus the time derivative reads:

$$\frac{\partial}{\partial t} = \frac{\partial}{\partial t_0} + \epsilon \frac{\partial}{\partial t_1} + \epsilon^2 \frac{\partial}{\partial t_2}. \quad (26)$$

The initial conditions are chosen as:

$$r_1(0, t_1, t_2; E) = \xi_0, \quad 0 < \xi_0 < 1; \quad r_{2,3,4}(0, t_1, t_2; E) = 0. \quad (27)$$

Now we proceed according to this plan: substitute the expansions (25) and (26) in Eq. (1), collect the terms of the same powers of ϵ on each of the two sides of the equation and equate them; next, for each of the resulting statements, collect the terms proportional to $\cos ky$, $\sin ky$, $\cos 2ky$, and $\sin 2ky$ on each of the two sides of a statement and equate, separately, the coefficients of these harmonics.

At the order ϵ we get:

$$\frac{\partial r_1}{\partial t_0} \cos ky + \frac{\partial r_4}{\partial t_0} \sin ky = \sigma(k; E) r_1 \cos ky + \sigma(k; E) r_4 \sin ky, \quad (28)$$

thus

$$\frac{\partial r_{1,4}}{\partial t_0} = \sigma(k; E) r_{1,4}, \quad (29)$$

where the growth rate $\sigma(k; E)$ is given by Eq. (4).

At the order ϵ^2 we get:

$$\frac{\partial r_1}{\partial t_1} \cos ky + \frac{\partial r_4}{\partial t_1} \sin ky + \frac{\partial r_2}{\partial t_0} \cos 2ky + \frac{\partial r_3}{\partial t_0} \sin 2ky = f_1(k, r_1, r_4; E) + f_2(k, r_1, r_4, r_2; E) \cos 2ky + f_3(k, r_1, r_4, r_3; E) \sin 2ky, \quad (30)$$

where $f_{1,2,3}$ are certain complicated functions. Therefore:

•

$$\frac{\partial r_{1,4}}{\partial t_1} = 0 \rightarrow r_{1,4} = r_{1,4}(t_0, t_2; E). \quad (31)$$

Applying the initial conditions (27) and accounting for Eq. (31) we get from the linear ODE (29):

$$r_1 = r_1(t_0; E) = \xi_0 e^{\sigma(k; E)t_0}, \quad r_4 = 0. \quad (32)$$

Here $\sigma(k; E) > 0$, since the case of unstable primary mode is of interest. It can be observed now that the LSA result of Sec. IIA for the primary mode has been obtained at the linear stage (at order ϵ) of a multi-scale expansion.

- Substituting $r_4 = 0$ in f_2 and f_3 , for r_2 and r_3 from Eq. (30) one obtains the linear ODEs:

$$\frac{\partial r_{2,3}}{\partial t_0} = f_{2,3}(k, r_1, r_{2,3}; E) = p(k; E)r_{2,3} + q_{2,3}(k; E)r_1(t_0; E)^2, \quad (33)$$

where

$$p(k; E) = 2 \frac{2 + S(1 + \cos 2\psi)}{1 + S} k^2 (1 - 4k^2) + 4E \frac{S \sin 2\psi}{1 + S} k^2 = \sigma(2k; E), \quad (34)$$

$$q_2(k; E) = -3 \frac{2 + S(1 + \cos 2\psi)}{4(1 + S)} k^2 (1 + k^2) - E \frac{S \sin 2\psi}{2(1 + S)} k^2, \quad (35)$$

$$q_3(k; E) = \frac{S \sin 2\psi}{1 + S} k^3 (1 - k^2) + E \frac{S^2(\cos 4\psi - 1) - S(6 \cos 2\psi + 10) - 12}{4(1 + S)} k^3. \quad (36)$$

Substituting $r_1(t_0; E)$ from Eq. (32) and taking into account the initial conditions, the solutions of Eqs. (33) read:

$$r_{2,3} = r_{2,3}(t_0; E) = \frac{q_{2,3}(k; E)\xi_0^2}{\sigma(2k; E) - 2\sigma(k; E)} [\exp(\sigma(2k; E)t_0) - \exp(2\sigma(k; E)t_0)]. \quad (37)$$

- Finally, for consistency of Eq. (30) one needs $f_1(k, r_1; E) = 0$. This gives the constraint $k^2(k^2 - k_c^2)r_1(t_0; E)^2 = 0$, where k_c is seen in Eq. (5). Since $r_1(t_0; E) \neq 0$, either $k = 0$, or $k = k_c$. We proceed below under assumption that the constraint holds approximately at $k = \delta_1$ and $k = k_c - \delta_2$, where $\delta_{1,2}$ are a positive constants that quantify the deviation from these values into the instability interval $0 < k < k_c$. In particular, $k = \delta_1$ is the most dangerous wavenumber in LSA when $\delta_1 = k_c/\sqrt{2}$.

Figure 6 shows r_1 as a function of the electric field at fixed t_0 and at various distances δ from the longwave instability threshold $k = 0$ and from the short-wave instability cut-off $k = k_c$. For this, we took $\delta_1 = \delta_2 = \delta$ and substituted $k = \delta$ and $k = k_c - \delta$ in Eq. (32), where $\sigma(k; E)$ and $k_c(E)$ are given by Eqs. (4), (5). In the former case (Fig. 6(b)) one can see that $r_1 \sim c_1 \exp(c_2 E)$, $c_1, c_2 = \text{const.}$, and values of these constants can be easily calculated. However, for the particular numerical values of the parameters and for the plotting interval these exponential curves are well approximated by the straight lines. In the latter case (Fig. 6(a)) the analytical dependence on E is complicated, but the curve data can be fitted: $\delta = 0.001$: $r_1 = 0.00997 + 0.000048 \exp(0.145717E)$; $\delta = 0.01$: $r_1 = 0.00973 + 0.000458 \exp(0.153945E)$; $\delta = 0.025$: $r_1 = 0.00941 + 0.001056 \exp(0.16734E)$.

A close look at $r_2(E)$ and $r_3(E)$ curves (Fig. 7) and the comparison to $r_1(E)$ in Fig. 6 shows, first, that r_1 is several orders of magnitude larger than $r_{2,3}$. Thus the primary mode $\cos ky$ is dominant in the spectrum, as expected [18]. Next, the absolute values of r_2 are two orders of magnitude larger than the absolute values of r_3 near the longwave instability threshold, while the converse is true near the short-wave instability cut-off. Therefore $\cos 2ky$ and $\sin 2ky$ are the next two fast growing modes in the spectrum.

The largest of $r_{2,3}$ amplitudes, r_3 , is plotted in Fig. 8 vs. t_0 and E near the short-wave instability cut-off. Cross-cutting Fig. 8(a) by a vertical cut shows that at any fixed t_0 the amplitude dependence on E is roughly as seen in Fig. 7(b). Moreover, a (positive) maximum of the amplitude increases with t_0 , as seen in Fig. 8(b).

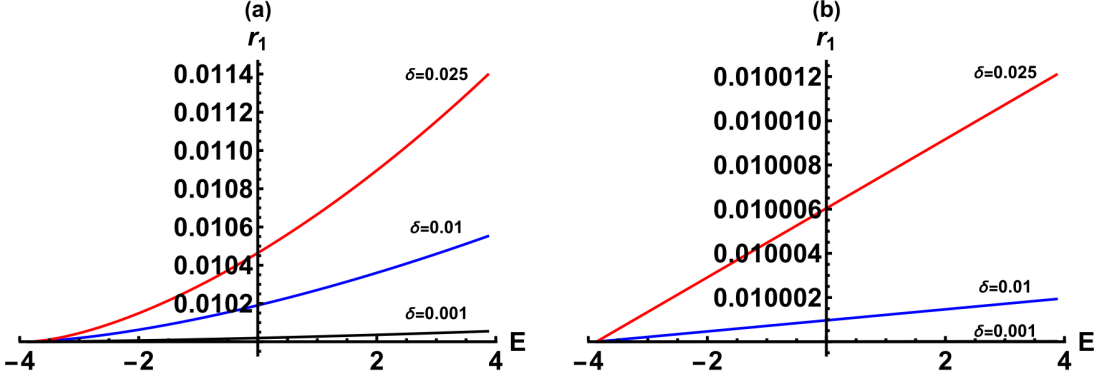


FIG. 6. The amplitude of $\cos ky$ term in the ansatz (25), given by Eq. (32), at $t_0 = 1$, $\xi_0 = 0.01$ for $E_c + 0.01 \leq E \leq -E_c$, where $E_c = -3.866$. (a) Near the short-wave instability cut-off; (b) Near the long-wave instability threshold.

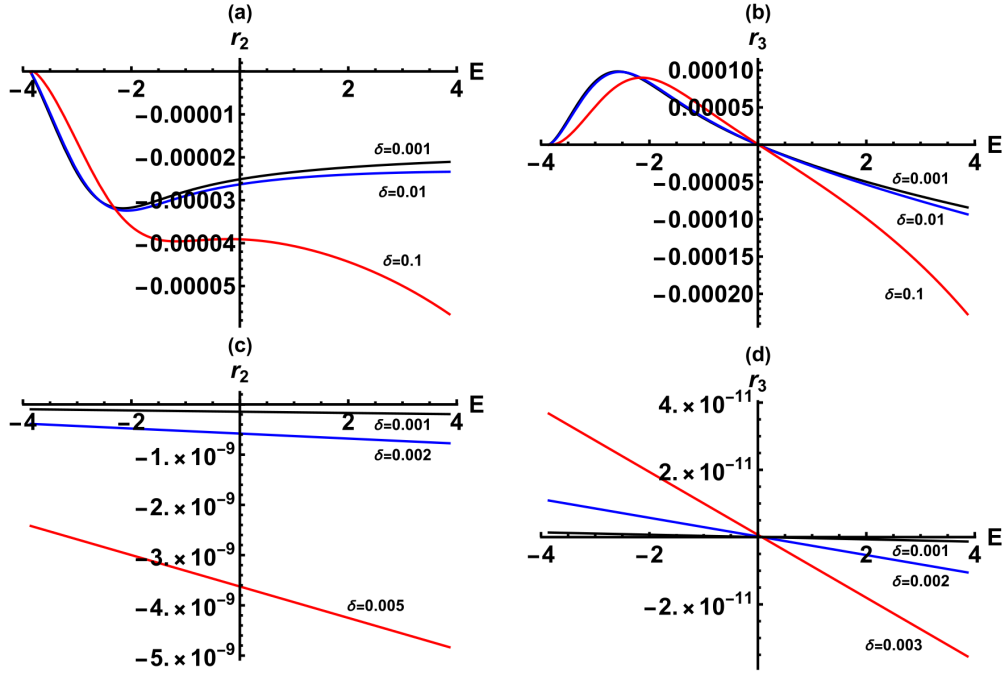


FIG. 7. The amplitudes of $\cos 2ky$ and $\sin 2ky$ terms in the ansatz (25), given by Eqs. (37), at $t_0 = 1$, $\xi_0 = 0.01$ for $E_c + 0.01 \leq E \leq -E_c$, where $E_c = -3.866$. (a,b) Near the short-wave instability cut-off; (c,d) Near the long-wave instability threshold.

V. SUMMARY

Provided that the electric field slightly exceeds a threshold value that is necessary for initiation of a morphological instability, the weakly nonlinear analysis that we carried out shows for the first time the electric field-and-time dependence of the dimensions of the focusing self-similar perturbation's amplitude profile approaching a blow-up. That amplitude singularity marks a wire pinch-off and its breakup into a chain of nanoparticles. In particular, this analysis shows that the amplitude initially grows quadratically in the deviation from a threshold value of the electric field. For the initial surface perturbation of the form $\xi_0 \cos ky$, $0 < \xi_0 < 1$ (where y is the axial variable) a separate, multi-scale analysis of a weakly nonlinear phase of the instability shows that in that regime the fastest growing instability modes are $\cos ky$, $\cos 2ky$, and $\sin 2ky$, and for these modes we found the explicit dependence of their amplitudes on time and the strength of the applied electric field.

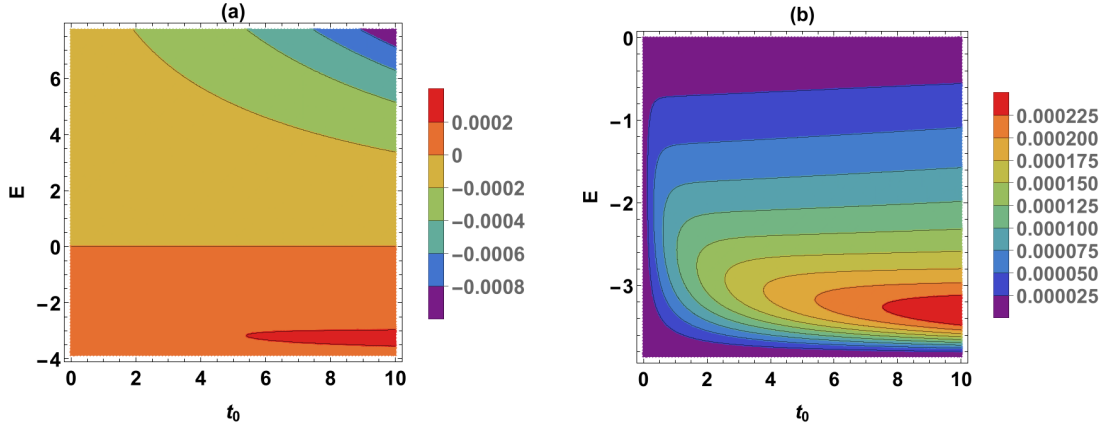


FIG. 8. The amplitude of $\sin 2ky$ term in the ansatz (25), given by Eqs. (37), at $\xi_0 = 0.01$, near the short-wave instability cut-off. (b) is the zoom view of the bottom region in (a).

VI. ACKNOWLEDGMENTS

The author thanks Alexander A. Nepomnyashchy and Mark R. Bradley for very useful suggestions and discussions regarding the analysis in Sec. III. Mark R. Bradley is also acknowledged for bringing his paper [23] to author's attention and for pointing to Ref. [28].

-
- [1] H.B. Huntington, Ch. 6: Electromigration in metals, in: *Diffusion in Solids: Recent Developments*, Ed. A.S. Nowick, Academic Press, 1975.
 - [2] P.S. Ho and T. Kwok, "Electromigration in metals", *Rep. Prog. Phys.* **52**, 301-348 (1989).
 - [3] P.J. Rous, T.L. Einstein, and E.D. Williams, "Theory of surface electromigration on metals: application to self-electromigration on Cu(111)", *Surf. Sci.* **315**, L995-L1002 (1994).
 - [4] Hongkun Park, Andrew K. L. Lim, A. Paul Alivisatos, J. Park, and Paul L. McEuen, "Fabrication of metallic electrodes with nanometer separation by electromigration", *Appl. Phys. Lett.* **75**, 301 (1999).
 - [5] L. Valladares, L.L. Felix, A.B. Dominguez, T. Mitrelias, F. Sfigakis, S.I. Khondaker, C.H.W. Barnes, and Y. Majima, "Controlled electroplating and electromigration in nickel electrodes for nanogap formation", *Nanotechnology* **21**, 445304 (2010).
 - [6] L. Arzubiaga, F. Golmar, R. Liopis, F. Casanova, and L.E. Hueso, "Tailoring palladium nanocontacts by electromigration", *Appl. Phys. Lett.* **102**, 193103 (2013).
 - [7] R. Hoffmann-Vogel, "Electromigration and the structure of metallic nanocontacts", *Appl. Phys. Rev.* **4**, 031302 (2017).
 - [8] F.A. Nichols and W.W. Mullins, "Surface-(Interface-) and volume-diffusion contributions to morphological changes driven by capillarity", *Trans. Metall. Soc. AIME* **233**, 1840-1848 (1965).
 - [9] F.A. Nichols and W.W. Mullins, "Morphological Changes of a Surface of Revolution due to Capillarity Induced Surface Diffusion", *J. Appl. Phys.* **36**, 1826 (1965).
 - [10] J.W. Cahn, "Stability of rods with anisotropic surface free energy", *Scripta Metall.* **13**, 1069-1071 (1979).
 - [11] A.J. Bernoff, A.L. Bertozzi, and T.P. Witelski, "Axisymmetric surface diffusion: dynamics and stability of self-similar pinchoff", *J. Stat. Phys.* **93** 725-776 (1998).
 - [12] B.D. Coleman, R.S. Falk, and M. Moakher, "Stability of cylindrical bodies in the theory of surface diffusion", *Physica D* **89**, 123-135 (1995).
 - [13] M.S. McCallum, P.W. Voorhees, M.J. Miksis, S.H. Davis, and H. Wong, "Capillary instabilities in solid thin films: Lines", *J. Appl. Phys.* **79**, 7604 (1996).
 - [14] H. Wong, M.J. Miksis, P.W. Voorhees, and S.H. Davis, "Universal pinch off of rods by capillarity-driven surface diffusion", *Scripta Mater.* **39**, 55-60 (1998).
 - [15] D.J. Kirill, S.H. Davis, M.J. Miksis, and P.W. Voorhees, "Morphological instability of a whisker", *Proc. R. Soc. Lond. A* **455**, 3825-3844 (1999).
 - [16] K.F. Gurski, and G.B. McFadden, "The effect of anisotropic surface energy on the Rayleigh instability", *Proc. R. Soc. Lond. A* **459** 2575-2598 (2003).
 - [17] K.F. Gurski, G.B. McFadden, and M.J. Miksis, "The effect of contact lines on the Rayleigh instability with anisotropic surface energy", *SIAM J. Appl. Math.* **66**, 1163-1187 (2006).

- [18] F. Wang, O. Tschukin, T. Leisner, H. Zhang, B. Nestler, M. Selzer, G.C. Marques, and J. Aghassi-Hagmann, “Morphological stability of rod-shaped continuous phases”, *Acta Materialia* **192**, 20-29 (2020).
- [19] V. Gorshkov and V. Pivman, “Kinetic Monte Carlo model of breakup of nanowires into chains of nanoparticles”, *J. Appl. Phys.* **122**, 204301 (2017).
- [20] M. Khenner, “Effect of electromigration on onset of morphological instability of a nanowire”, *J. Eng. Math.* **140**, 6 (2023).
- [21] M. Khenner, “Nanowire breakup via a morphological instability enhanced by surface electromigration”, *Modelling and Simulation in Materials Science and Engineering* **32**, 015003 (2024).
- [22] T.F. Marinis, R.F. Sekerka, F.D. Lemkey, H.E. Cline, and M. McLean, In-Situ Composites IV, Elsevier, NY, pp. 315-327 (1982).
- [23] M.P. Gelfand and R.M. Bradley, “One dimensional conservative surface dynamics with broken parity: Arrested collapse versus coarsening”, *Physics Letters A* **379**, 199–205 (2015).
- [24] S. Xu, P.F. Li, and Y. Lu, “In situ atomic-scale analysis of Rayleigh instability in ultrathin gold nanowires”, *Nano Res.* **11**, 625 (2018).
- [25] S. Karim, M.E. Toimil-Molaes, A.G. Balogh, W. Ensinger, T.W. Cornelius, E.U. Khan, and R. Neumann, “Morphological evolution of Au nanowires controlled by Rayleigh instability”, *Nanotechnology* **17**, 5954–5959 (2006).
- [26] M. Schimschak and J. Krug, “Surface electromigration as a moving boundary value problem”, *Phys. Rev. Lett.* **78**, 278 (1997).
- [27] R.M. Bradley, private communication.
- [28] A.J. Bernoff and A.L. Bertozzi, “Singularities in a modified Kuramoto-Sivashinsky equation describing interface motion for phase transition”, *Physica D* **85**, 375-404 (1995).
- [29] A.J. Bernoff and T.P. Witelski, “Stability and dynamics of self-similarity in evolution equations”, *J. Eng. Math.* **66**, 11-31 (2010).